Analysis of OFDM signals for ranging and communications

Andrew M. Graff*, William N. Blount*, Peter A. Iannucci*, Jeffrey G. Andrews†, and Todd E. Humphreys*

*Radionavigation Laboratory, †Department of Electrical and Computer Engineering
The University of Texas at Austin

BIOGRAPHIES

Andrew M. Graff (BS, Electrical and Computer Engineering, The University of Texas at Austin) is a PhD student in the Department of Electrical and Computer Engineering at The University of Texas at Austin and a member of the Radionavigation Laboratory. His research interests are in sensing systems to enable robust positioning and wireless communications.

William N. Blount (BS, Mathematics, Electrical and Computer Engineering, The University of Texas at Austin) is a PhD student in the Department of Electrical and Computer Engineering at The University of Texas at Austin and a member of the Radionavigation Laboratory. His research interests are in the intersection of satellite telecommunications, PNT, and large multi-antenna systems.

Peter A. Iannucci (BS, Electrical Engineering-Computer Science and Physics, MIT; PhD, Networks and Mobile Systems, CSAIL, MIT) is a postdoctoral research fellow in the Radionavigation Laboratory at The University of Texas at Austin, and a member of the UT Wireless Networking and Communications Group (WNCG). His current research interests include collaborative navigation, multi-spectral mapping, and re-purposing broadband Internet satellites for radionavigation.

Jeffrey Andrews (BS, Engineering, Harvey Mudd College; MS, PhD, Electrical Engineering, Stanford University) is the Cockrell Family Endowed Chair in Engineering at the University of Texas at Austin where he is Director of 6G@UT. He received the 2015 Terman Award, the NSF CAREER Award, and the 2019 IEEE Kiyo Tomiyasu technical field award. Dr. Andrews is an ISI Highly Cited Researcher and has been co-recipient of 15 best paper awards. He is an IEEE Fellow. His research is focused on wireless communication systems.

Todd Humphreys (BS, MS, Electrical Engineering, Utah State University; PhD, Aerospace Engineering, Cornell University) is a professor in the department of Aerospace Engineering and Engineering Mechanics at The University of Texas at Austin, where he directs the Radionavigation Laboratory. He specializes in the application of optimal detection and estimation techniques to problems in secure, collaborative, and high-integrity perception, with an emphasis on navigation, collision avoidance, and precise timing. His awards include The University of Texas Regents' Outstanding Teaching Award (2012), the National Science Foundation CAREER Award (2015), the Institute of Navigation Thurlow Award (2015), the Qualcomm Innovation Fellowship (2017), the Walter Fried Award (2012, 2018), and the Presidential Early Career Award for Scientists and Engineers (PECASE, 2019). He is a Fellow of the Institute of Navigation and the Royal Institute of Navigation.

ABSTRACT

This paper analyzes the precision bounds of ranging (via time-of-arrival estimation) with OFDM signals and proposes methods for the co-design of OFDM waveforms meeting both ranging and communication goals. First, it presents a method for obtaining an upper bound for the channel capacity and a lower bound for the ranging variance of an OFDM system as a function of the OFDM parameters and channel model. Next, it introduces an analysis tool that implements this method, allowing for numerical computation of the communications capacity and ranging variance bounds from OFDM parameters. Finally, it presents a general analysis, expressed in terms of channel capacity and ranging variance, of the trade-offs associated with varying various OFDM parameters.

Preprint of the 2021 ION GNSS+ Conference St. Louis, Sept. 20-24, 2021

INTRODUCTION

Wireless communication networks serve numerous mobile, vehicular, and aerospace needs. Orthogonal frequency-division multiplexing (OFDM) is by far the modulation of choice for these systems, with widespread adoption in standards such as 802.11, long term evolution (LTE), and 5G new radio (NR). But communication is not sufficient for next-generation wireless networks: both as an enabler of efficient physical-layer operation and as a key component of application-layer services, these networks increasingly demand precise positioning. To meet this demand, there is increasing interest in extracting ranging estimates from communications signals to provide or supplement user localization. The precision of such ranging estimates is a secondary design consideration in wireless communication standards: data rate, latency, and reliability are, quite naturally, the standards' primary concerns. But with the increasing importance of within-network localization, the time is right to consider the co-design of OFDM waveforms for both ranging and communications.

This paper employs the Ziv-Zakai bound to quantify the ranging precision of generic OFDM waveforms, with the intent that this bound can both enable comparison between existing OFDM standards and guide the design of forthcoming waveforms. To support the design of new waveforms, this paper will additionally explore the tradeoffs between ranging precision and data rate with respect to various OFDM design parameters.

OFDM's widespread adoption and popularity in digital communications standards makes it a prime candidate for positioning applications. Existing communications standards, particularly LTE and 5G NR, include protocols tailored specifically for location-based services. The precision requirements of these positioning protocols are becoming increasingly demanding, so much so that 3GPP, the body that defines cellular standards, has acknowledged the need for further enhancements in the 5G NR protocol to meet desired localization accuracy requirements [1]. Meanwhile, positioning requirements are constantly being pushed to new limits to enable groundbreaking applications in vehicular safety, autonomous coordination, and beyond.

OFDM can offer excellent ranging performance: Wang et al. concluded that, under certain configurations, OFDM signals can be superior to pseudo-noise (PN) signals for time-based range estimation [2], opening the possibility that OFDM-based positioning solutions could outperform existing PN-based systems such as GNSS.

To enable design of new OFDM waveforms to meet both communications and ranging goals, a thorough understanding of the feasible ranging precision of generic OFDM signals is essential. The fundamental ranging precision of a signal can be derived from its autocorrelation function (ACF). The ACF of an OFDM signal at baseband, however, may contain problematic sidelobes that can cause range ambiguities when the signal-to-noise ratio (SNR) falls below a certain threshold. Whereas this thresholding effect is not captured by the Cramer-Rao Lower Bound (CRLB), it is captured by the Ziv-Zakai [3] bound.

OFDM signals in communications systems often contain a preamble, which acts as a known reference for synchronization and channel estimation, followed by data blocks. Within these data blocks, known training symbols may be transmitted on a subset of the subcarriers, called pilots, to further aid in channel estimation and tracking. The signal in the preamble is often chosen as a sequence with desirable autocorrelation properties such as a Zadoff-Chu or other constant-amplitude-zero-autocorrelation waveform. These are desirable because they have an out-of-phase autocorrelation equal to zero. By contrast, the ACF of the data blocks enjoys no such purposeful design, and may exhibit undesirable sidelobes. Parameters such as the number of pilots, the pilot subcarrier locations, and the pilot's complex-valued symbols all affect the ACF, as manifested in different mainlobe widths, sidelobe amplitudes, and sidelobe positions. Prior work has analyzed how changes in these parameters affect the sidelobe energy in the OFDM ACF [4], but not the impact that the sidelobe energy has on parameter estimation or ranging. The present paper will compute the Ziv-Zakai bound to quantify the impact that such OFDM parameters have on ranging precision.

Much prior work has analyzed the positioning capabilities of OFDM signals, but only within the framework of existing communication protocols. This work is extensive and covers analysis of different time-of-arrival estimators for LTE [5], studies of positioning accuracy in 5G NR [1], and opportunistic positioning using LTE [6], [7], FM OFDM [8], and mobile TV [9] signals. Besides limiting itself to existing protocols, these works also focus primarily on simulated or experimental results and do not address the specific design of the OFDM signal. Driusso et al. partially addressed signal design and studied how the placement of positioning pilots within the LTE framework affected ranging performance by computing the Ziv-Zakai bound [10]. But, while insights regarding subcarrier placement are valuable for the design of OFDM waveforms for ranging, the restriction to only signals achievable within LTE limits that study's applicability. Furthermore, the bounds discovered in [10] do not account for fading effects, which are common and known to

degrade ranging performance. Wang et al. provided ranging accuracy bounds for a generic OFDM signal model that included multipath fading but only computed the CRLB, failing to address the SNR threshold effect, which will not be uncommon in OFDM-based ranging [11]. The present paper will model a generic OFDM signal so that the ranging precision of any OFDM-type waveform may quantified. It will also go beyond the aforementioned works by modeling fading and capturing the SNR threshold effect inherent to OFDM ranging.

The communication capacity of OFDM systems has also been extensively studied in prior work. Goldsmith's textbook on wireless communications thoroughly covers the computation of channel capacity in the presence of fading [12]. Yoo and Goldsmith extended this analysis to MIMO channels that have channel estimation error [13]. Tang et al. analyzed the effect of channel estimation error in the presence of Rayleigh fading [14]. Ohno provided analysis on the MMSE channel estimation error in OFDM systems and its impact on channel capacity in block Rayleigh fading [15]. Ohno used this work to propose optimal pilots to maximize capacity. While the capacity of these systems alone has been thoroughly analyzed, such analysis has not been combined with a ranging precision analysis to illuminate the trade-offs between capacity and ranging accuracy.

This paper will address the tradeoff between ranging precision and communications data throughput with regard to various OFDM design parameters. One may anticipate that an OFDM signal which is optimal for ranging may not be optimal for communications, and vice versa: if more time-frequency resources must transmit pilots to meet ranging precision requirements, fewer resources remain for data transmission. Requirements may also be imposed on other fundamental parameters such as the subcarrier quantity, subcarrier spacing, pilot power allocation, and bandwidth. In the design of multi-functional systems which may demand both high data-rate communications and precise positioning, understanding the governing tradeoffs is crucial for efficient utilization of the available spectrum.

Contributions

This paper's contributions are threefold: (1) an analysis tool that takes system and OFDM signal parameters as inputs and provides both an upper bound on communication capacity and a lower bound on ranging variance as output, (2) an analysis of the trade-off in these two output values as certain OFDM parameters are varied, and (3) suggestions and examples of how these results can be used to design an OFDM signal for a given propagation environment that achieves a required capacity and ranging variance.

Notation

The following notation will be used throughout this paper. Column vectors are denoted with lowercase bold $\boldsymbol{x}$. Matrices are denoted with uppercase bold $\boldsymbol{X}$. Scalars are denoted without bold x. The ith entry of a vector $\boldsymbol{x}$ is designated as $x[i]$. Real transpose is represented by superscript T and conjugate transpose is represented by superscript H.

SIGNAL MODEL

A user is assumed to receive an OFDM signal that has propagated through a finite-impulse-response (FIR) channel in the presence of additive white Gaussian noise (AWGN). The signal model is discrete time and baseband. The OFDM system operates with K subcarriers and a cyclic-prefix length of L_c. Let $(s_m[k])_{k=0}^{K-1}$ be the complex symbol sequence for the m^{th} OFDM symbol. These are modulated onto subcarriers using an inverse Fourier transform, creating a complex time-domain signal with $\bar{K} = K + L_c$ samples per OFDM symbol. Suppose M OFDM symbols are transmitted. Then the transmitted signal is

$$w[n] = \frac{1}{K} \sum_{k=0}^{K-1} s_m[k] e^{j2\pi \frac{k(q-L_c)}{K}}, \quad m = \lfloor n/\bar{K} \rfloor, \quad q = n \bmod \bar{K}, \quad n = 0, 1, \ldots, M\bar{K} - 1. \tag{1}$$

The first sample of the m^{th} OFDM symbol is $w[m\bar{K}]$. The time-domain signal propagates through a fading channel modeled as an L-order finite impulse response (FIR) filter with $\bar{L} = L + 1$ taps $(h[l])_{l=0}^{L}$. The signal is also subject to noise modeled as AWGN and expressed as the sequence $(v[n])_{n=0}^{M\bar{K}-1}$, where $v[n] \sim \mathcal{CN}(0, \sigma_v^2)$. It is assumed that $\bar{L} \leq L_c$. The resulting received signal is given by

$$y[n] = \sum_{l=0}^{L} h[l] w[n-l] + v[n], \quad n = 0, 1, \ldots, M\bar{K} - 1. \tag{2}$$

Three channel types are considered: (1) an AWGN channel for which $L = 0$ and $h[0] = g$, where g is a deterministic gain; (2) a Rayleigh frequency-flat channel, for which $L = 0$ and $h[0] \sim \mathcal{CN}(0, \sigma^2_{h[0]})$; and (3) a Rayleigh frequency-selective channel, for which $L \geq 1$ and $h[l] \sim \mathcal{CN}(0, \sigma^2_{h[l]})$ for $l = 0, 1, \ldots, L$.

Channel Capacity

The approach to computing the channel capacity is motivated by [15], which considers channel estimation error present in the minimum-mean-squared-error (MMSE) channel coefficients estimator. This estimation error factors into the communication link's effective SNR.

Assume that for the m^{th} OFDM symbol, pilot subcarriers are placed at indices $I_b^{(m)}$ and data subcarrier are placed at indices $I_s^{(m)}$ such that these sets are disjoint and exhaustive: $I_b^{(m)} \cup I_s^{(m)} = \{k : k \in [1, K]\}$. Define the pilot vector $\tilde{\boldsymbol{b}}^{(m)} \in \mathbb{R}^K$ such that $\tilde{b}^{(m)}[k] = s_m[k]$ for $k \in I_b^{(m)}$ and $\tilde{b}^{(m)}[k] = 0$ otherwise. Let $\boldsymbol{F}$ be a $K \times K$ discrete Fourier transform (DFT) matrix. The DFT of $\tilde{\boldsymbol{b}}^{(m)}$ is $\boldsymbol{b}^{(m)} = \boldsymbol{F}\tilde{\boldsymbol{b}}^{(m)}$. Let $\boldsymbol{B}^{(m)} \in \mathbb{R}^{K \times \bar{L}}$ be a Toeplitz matrix whose i^{th} column is equal to $\boldsymbol{b}^{(m)}$ circularly shifted by i samples. This circular shift accounts for the effect of the cyclic prefix. Disregarding the cyclic prefix samples, the portion of the received signal from the pilots is then $\boldsymbol{x}^{(m)} = \boldsymbol{B}^{(m)}\boldsymbol{h} + \boldsymbol{v}$. This system can be generalized to multiple OFDM symbols by defining $\boldsymbol{B} = [{\boldsymbol{B}^{(0)}}^T, ..., {\boldsymbol{B}^{(M)}}^T]^T$.

Assume the channel covariance $\boldsymbol{R}_h = \text{diag}([\sigma^2_{h[0]}, ..., \sigma^2_{h[\bar{L}]}])$, and define $\boldsymbol{R}_x = \boldsymbol{B}\boldsymbol{R}_h\boldsymbol{B}^H + \sigma_v^2\boldsymbol{I}$ and $\boldsymbol{R}_{hx} = \boldsymbol{R}_h\boldsymbol{B}^H$. Then the linear-minimum-mean-squared-error (LMMSE) estimate of $\boldsymbol{h}$ is $\hat{\boldsymbol{h}} = \boldsymbol{R}_{hx}{\boldsymbol{R}_x}^{-1}\boldsymbol{x}$ and its error covariance is $\boldsymbol{\Sigma} = \left({\boldsymbol{R}_h}^{-1} + \frac{1}{\sigma_v^2}\boldsymbol{B}^H\boldsymbol{B}\right)^{-1}$. Letting $\boldsymbol{F}_{\bar{L}}$ represent the first $\bar{L}$ columns of $\boldsymbol{F}$, and $\boldsymbol{f}_{\bar{L},i}^T$ the i^{th} row of $\boldsymbol{F}_{\bar{L}}$, the channel estimation error at subcarrier i is given by

$$E_i = K\boldsymbol{f}_{\bar{L},i}^H\boldsymbol{\Sigma}\boldsymbol{f}_{\bar{L},i}. \tag{3}$$

Define the total channel power as $\sigma_H^2 = \text{trace}(\boldsymbol{R}_h)$. Also define the average received pilot power during symbol m as $P_b^{(m)}$ and the average received data power during symbol m as $P_s^{(m)}$. Let $\left|I_s^{(m)}\right|$ represent the number of subcarriers in $I_s^{(m)}$, i.e. those being used for data. As given by [15, eq. (27)] The effective data SNR at subcarrier $k \in I_s^{(m)}$ during symbol m is defined as

$$\rho_k^{(m)} = \frac{\sigma_H^2 - E_k}{E_k + \left|I_b^{(m)}\right| \sigma_v^2 / P_s^{(m)}}. \tag{4}$$

Now define the probability distribution function (pdf) of the SNR as $p_\gamma(\gamma)$. For AWGN, $p_\gamma(\gamma)$ is the dirac-delta function centered at 1. This indicates a deterministic and constant SNR. For Rayleigh fading, the distribution of SNR on each channel path is exponentially distributed. Therefore, the SNR γ of the maximum-ratio combining of each channel tap is the sum of exponentials. If all taps are assumed to have the same variance, that is $\sigma_h[l]^2 = \sigma_h^2$, then the SNR γ is distributed according to an Erlang-$\bar{L}$ distribution with parameter $\bar{\gamma_e}$, the average SNR on each channel tap. An Erlang-$\bar{L}$ distribution with parameter $\bar{\gamma_e}$ is equivalent to a Gamma$(\bar{L}, \bar{\gamma_e})$ distribution. By the scaling property, if $X \sim$ Gamma$(\bar{L}, 1/\bar{L})$, then $\bar{\gamma}X \sim$ Gamma$(\bar{L}, \bar{\gamma_e})$, where the mean of the distribution is $\bar{\gamma} = \bar{L}\bar{\gamma_e}$. The Shannon capacity of a channel can be computed from [12, eq. (4.7)]. The capacity is computed for each subcarrier assuming a unit bandwidth, summed over all subcarriers, and then divided by $M\bar{K}$ to give the capacity in units of bits-per-second-per-hertz (bps/Hz). This channel capacity is defined as

$$C = \frac{1}{M\bar{K}} \sum_{m=0}^{M} \sum_{k \in I_s^{(m)}} \int_0^\infty \log_2(1 + \rho_k^{(m)}\gamma) p_\gamma(\gamma) d\gamma. \tag{5}$$

Ranging Variance

The Ziv-Zakai bound will be used to bound the system's ranging variance. The Ziv-Zakai bound is a lower bound on the variance of an unbiased estimator. For the purposes of this paper, the time-of-arrival (ToA) of a signal is being estimated. Denote the ToA as τ, the variance of the estimator as $\bar{\epsilon}^2$, and the Ziv-Zakai bound itself as ZZB, such that $\bar{\epsilon}^2 \geq$ ZZB. First, a binary detection problem is examined where two hypothesis are equally likely: the received signal experienced delay τ, or the received signal experienced delay $\tau + z$. Then $P_{min}(z)$ is defined to be the probability of

error of the optimal detector. If a priori knowledge that the ToA is uniformly distributed in $[0, T_a]$ is assumed, then the Ziv-Zakai bound can be given by [3], [16]

$$\text{ZZB} = \frac{1}{T_a}\int_0^{T_a} z(T_a - z)P_{min}(z)dz. \tag{6}$$

The derivations P_{min} for the different fading types will now be explored. First consider AWGN, where the received signal is given by $\boldsymbol{x} = \boldsymbol{b} + \boldsymbol{v}$. Let us consider a new representation of the signal where the real and imaginary components are separated: $\boldsymbol{y} = \boldsymbol{\mu} + \boldsymbol{\eta}$, $\boldsymbol{\mu} = [\text{real}(\boldsymbol{b})\ \text{imag}(\boldsymbol{b})]^T$, and $\boldsymbol{\eta} = [\text{real}(\boldsymbol{v})\ \text{imag}(\boldsymbol{v})]^T$. The noise variance is given by $\sigma_\eta^2 = \frac{\sigma_v^2}{2}$. The pdf for this signal $\boldsymbol{y}$ is given by

$$p(\boldsymbol{y}|\tau) = \frac{exp(-\frac{1}{\sigma_v^2}(\boldsymbol{y}-\boldsymbol{\mu})^T(\boldsymbol{y}-\boldsymbol{\mu}))}{\sqrt{(\sigma_v^2\pi)^{2N}}}. \tag{7}$$

Again, assume that the signal has experienced a delay of τ. Without loss of generality, assume τ is zero. Let us accordingly denote the signal mean as $\boldsymbol{\mu_0}$, denoting no shift. Then the corresponding signal for the second hypothesis with additional delay z will be equivalently defined, but with mean $\boldsymbol{\mu_z}$, indicating a circular shift of $\boldsymbol{\mu_0}$ by z samples. The likelihood ratio between these two signal is then given by

$$\Lambda = \frac{p(\boldsymbol{y}|\tau)}{p(\boldsymbol{y}|\tau + z)}. \tag{8}$$

The detection rule is $\Lambda > 1$. The detector can be simplified as follows:

$$\log\Lambda > 0 \tag{9}$$

$$-\frac{1}{\sigma_v^2}(\boldsymbol{y}-\boldsymbol{\mu_0})^T(\boldsymbol{y}-\boldsymbol{\mu_0}) + -\frac{1}{\sigma_v^2}(\boldsymbol{y}-\boldsymbol{\mu_z})^T(\boldsymbol{y}-\boldsymbol{\mu_z}) > 0 \tag{10}$$

$$-\boldsymbol{y}^T\boldsymbol{y} + 2\boldsymbol{y}^T\boldsymbol{\mu_0} - \boldsymbol{\mu_0}^T\boldsymbol{\mu_0} + \boldsymbol{y}^T\boldsymbol{y} - 2\boldsymbol{y}^T\boldsymbol{\mu_z} + \boldsymbol{\mu_z}^T\boldsymbol{\mu_z} > 0 \tag{11}$$

$$\boldsymbol{y}^T\boldsymbol{\mu_0} - \boldsymbol{y}^T\boldsymbol{\mu_z} > 0 \tag{12}$$

$$\boldsymbol{y}^T(\boldsymbol{\mu_0} - \boldsymbol{\mu_z}) > 0 \tag{13}$$

Now assume that the first hypothesis is true: $\boldsymbol{y} = \boldsymbol{\mu_0} + \boldsymbol{\eta}$.

$$(\boldsymbol{\mu_0} + \boldsymbol{\eta})^T(\boldsymbol{\mu_0} - \boldsymbol{\mu_z}) > 0 \tag{14}$$

$$\boldsymbol{\eta}^T(\boldsymbol{\mu_0} - \boldsymbol{\mu_z}) > \boldsymbol{\mu_0}^T\boldsymbol{\mu_0} - \boldsymbol{\mu_0}^T\boldsymbol{\mu_z} \tag{15}$$

Recognize that $\boldsymbol{\mu_0}^T\boldsymbol{\mu_0}$ is the autocorrelation of $\boldsymbol{\mu_0}$ evaluated at 0 and $\boldsymbol{\mu_0}^T\boldsymbol{\mu_z}$ is the autocorrelation of $\boldsymbol{\mu_0}$ evaluated at z. Denote the autocorrelation function of $\boldsymbol{\mu_i}$ as $a[i]$. Also recognize that $\boldsymbol{\eta}^T(\boldsymbol{\mu_0} - \boldsymbol{\mu_z})$ is a linear combination of jointly-distributed Gaussians. As a result, $\boldsymbol{\eta}^T(\boldsymbol{\mu_0} - \boldsymbol{\mu_z})$ is distributed as a Gaussian with zero mean and a variance of

$$\frac{\sigma_v^2}{2}\sum_{j=1}^{2N}(\mu_0[j] - \mu_z[j])^2. \tag{16}$$

Therefore, probability of error for the detection rule can be rewritten as

$$P_{min}(z) = Q\left(\frac{a[0] - a[z]}{\frac{\sigma_v}{\sqrt{2}}\sqrt{\sum_{j=1}^{2N}(\mu_0[j] - \mu_z[j])^2}}\right). \tag{17}$$

For the Rayleigh multipath case, a similar derivation can be followed. Assume that the channel is perfectly known and that same maximum-ratio combining gains that were seen in the capacity computation are seen here as well. As such, the channel-corrected signal can be described as $\boldsymbol{y} = \sqrt{\gamma}\boldsymbol{\mu} + \boldsymbol{\eta}$. By following an identical derivation:

$$P_{min}(z|\gamma) = Q\left(\sqrt{\gamma}\frac{a[0]-a[z]}{\frac{\sigma_v}{\sqrt{2}}\sqrt{\sum_{j=1}^{2N}(\mu_0[j]-\mu_z[j])^2}}\right). \tag{18}$$

$$P_{min}(z) = \int_0^\infty Q\left(\sqrt{\gamma}\frac{a[0]-a[z]}{\frac{\sigma_v}{\sqrt{2}}\sqrt{\sum_{j=1}^{2N}(\mu_0[j]-\mu_z[j])^2}}\right) p_\gamma(\gamma)d\gamma. \tag{19}$$

Much like in the capacity computation, assume that $\gamma \sim \text{Gamma}(\bar{L}, \bar{\gamma}_e)$. So $P_{min}(z)$ is expressed as an integral over the fading distribution. This probability of error can then be substituted into the original equation for the Ziv-Zakai bound on ranging variance.

Additional Sub-optimal Derivations

So far, the derivations for the Ziv-Zakai bound depended entirely on the assumption that the channel knowledge is perfect. In this section, some novel derivations are explored in the case where there is no channel knowledge whatsoever. In this situation, assume that the user cross-correlates their perfect copy of the transmitted signal against the incoming signal which has been corrupted by the channel and noise. This differs from the previous case where the channel impairments were corrected prior to correlation. To use the Ziv-Zakai bound for this scenario, a new expression for $P_{min}(z)$ must be derived.

First, a probability distribution for the correlation function is derived. Recall the previous channel model $\boldsymbol{x} = \boldsymbol{B}\boldsymbol{h} + \boldsymbol{v}$. For now, only a single symbol is considered. A small modification to the matrix $\boldsymbol{B}$ will be made. Circularly shift $\boldsymbol{B}$ in the column direction by $1 + L/2$ samples to account for channel delay and treat the channel as non-causal. This is done to treat the true delay τ as the center channel tap. Now define a new matrix $\boldsymbol{B}_c \in \mathbb{R}^{K\times K}$ as a toeplitz matrix where the i^{th} column is equal to conj($\boldsymbol{b}$) circularly shifted by i samples. The circular correlation function can then be described as

$$\boldsymbol{a} = \boldsymbol{B}_c(\boldsymbol{B}\boldsymbol{h} + \boldsymbol{v}) = \boldsymbol{B}_c\boldsymbol{B}\boldsymbol{h} + \boldsymbol{B}_c\boldsymbol{v} \tag{20}$$

Now since no channel knowledge is assumed, the channel $\boldsymbol{h}$ has a zero-mean Gaussian distribution. Denote the channel covariance matrix as $\boldsymbol{\Sigma}_h$ and the noise covariance matrix as $\boldsymbol{\Sigma}_v$. Since $\boldsymbol{a}$ is a linear operation of a multivariate Gaussian, and $\boldsymbol{h} \perp\!\!\!\perp \boldsymbol{v}$, $\boldsymbol{a} \sim \mathcal{CN}(\boldsymbol{0}, \boldsymbol{\Sigma}_a)$, where

$$\boldsymbol{\Sigma}_a = \boldsymbol{B}_c\boldsymbol{B}\boldsymbol{\Sigma}_h\boldsymbol{B}^H\boldsymbol{B}_c^H + \boldsymbol{B}_c\boldsymbol{\Sigma}_v\boldsymbol{B}_c^H \tag{21}$$

Deriving the optimal detector based off of the likelihood ratio would be very challenging for this Gaussian, because its elements are correlated and the covariance matrix changes with the delay. Specifically, the covariance matrix is circularly shifted by z samples in both axis. Instead, the probability of error for a sub-optimal detector is analyzed. In this detector, hypothesis 0 is selected if the square of the correlation at delay 0 is greater than the square of the correlation at delay z, or $|a[0]|^2 > |a[z]|^2$. The probability of error then becomes

$$P_{min}(z) = P(|a[0])|^2 > |a[z]|^2) = P(|a[z]|^2 - |a[0]|^2 < 0) \tag{22}$$

This quantity will be calculated by finding the pdf of $|a[z]|^2 - |a[0]|^2$ and recognizing that (22) is the associated cumulative distribution function (cdf) evaluated at 0. Since $a[n]$ is a complex Gaussian,

$$|a[n]|^2 = |\text{real}(a[n])|^2 + |\text{imag}(a[n])|^2 = \frac{\sigma^2_{a[n]}}{2}X \tag{23}$$

$$X \sim \chi^2(2) \tag{24}$$

By the relation between chi-squared and gamma distributions, as well as the gamma scaling property:

$$|a[n]|^2 \sim \text{Gamma}(1, \sigma^2_{a[n]}) \tag{25}$$

Now, the distribution of $|a[z]|^2 - |a[0]|^2$ is particularly challenging, because the distributions are correlated. However, prior work was found that derived the distribution for correlated gamma random variables [17]. Define 2 random variables $X_1 \sim$ gamma(k, θ_1) and $X_2 \sim$ gamma(k, θ_2), where k is a common shape parameter and θ_1 and θ_2 are scale parameters. Also define the correlation coefficient between X_1 and X_2 as ρ. The pdf of the gamma difference distribution $\Delta = X_1 - X_2$ is given by

$$\begin{aligned} p_\Delta(\delta) = &\left(\frac{|\delta|^{k-0.5}}{\Gamma(k)\sqrt{\pi}\sqrt{\theta_1\theta_2(1-\rho)}} \right) \\ &\times \left(\frac{1}{(\theta_1+\theta_2)^2 - 4\theta_1\theta_2\rho} \right)^{\frac{2k-1}{4}} \\ &\times \exp\left(\left(\frac{\frac{\delta}{2}}{1-\rho} \right) \left(\frac{1}{\theta_2} - \frac{1}{\theta_1} \right) \right) \\ &\times K_{k-0.5}\left(|\delta| \frac{\sqrt{(\theta_1+\theta_2)^2 - 4\theta_1\theta_2\rho}}{2\theta_1\theta_2(1-\rho)} \right) \end{aligned} \tag{26}$$

when $\delta \neq 0$, and

$$p_\Delta(\delta) = \left(\frac{\Gamma(k-0.5)}{\sqrt{\pi}\Gamma(k)} \right) \left(\frac{(4\theta_1\theta_2(1-p))^{k-1}}{((\theta_1+\theta_2)^2 - 4\theta_1\theta_2 p)^{k-0.5}} \right) \tag{27}$$

when $\delta = 0$, assuming that $k \geq 1/2$. $K_n(.)$ is the modified Bessel function of the 2nd kind. The CDF of this distribution can be computed numerically. Now the correlation coefficient ρ must be determined. From [18], the correlation coefficient is the square of the correlation coefficient between the Gaussians before squaring. As a result, the correlation between $a[i]$ and $a[j]$ can be given by

$$\rho_{ij} = \frac{|(\mathbf{\Sigma}_a)_{ij}|^2}{(\mathbf{\Sigma}_a)_{ii}(\mathbf{\Sigma}_a)_{jj}}. \tag{28}$$

Now that an expression for the pdf has been defined, P_{min} can be calculated as

$$P_{min}(z) = P(|a[z]|^2 - |a[0]|^2 < 0) = \int_{-\infty}^{0} p_\Delta(\delta) d\delta. \tag{29}$$

Using this sub-optimal detector, the Ziv-Zakai bound can attempt to capture how poor the system's ranging performance becomes if the channel is entirely unknown. However, it is worth noting that due to the sub-optimality of the detector, these results are no longer a true lower-bound. The true lower-bound would require deriving the probability of error from the likelihood ratio test, which is reserved for future work.

ANALYSIS

A set of MATLAB modules were developed implementing both the capacity bound in (5) and the Ziv-Zakai ranging variance bound in (6). The modules share a common input definition, which fully define the OFDM signal and the system environment. These parameters are shown in Table I.

TABLE I: Table of parameters in the MATLAB modules

Parameters	**Default Value**
# subcarriers	64
# symbols	1
bandwidth	20 MHz
pilot placement	Every other subcarrier
pilot modulation	1
data power	SNR/2
pilot power	SNR/2
noise power	1 dBm
channel order	order 0
channel covariance	1
fading mode ("rayleigh" or "awgn")	awgn
channel knowledge ("perfect" or "none")	perfect
oversampling factor	64
oversampling filter	16-sample truncated sinc

The parameters in this system are chosen to loosely model an 802.11a WiFi system. This systems has $K = 64$ subcarriers and a bandwidth of $20\,\mathrm{MHz}$, resulting in subcarrier spacing of $0.3125\,\mathrm{MHz}$. The modules use an over sampling rate of $N_{os} = 64$ with oversampling performed by filtering with a truncated sinc spanning 16 samples in the original sampling rate. The remaining parameters are varied to study their impact on capacity and ranging variance through various tradeoff plots.

First, the system is examined using the default pilot placement. The communication capacity of the default system will be analyzed as a function of average SNR and of fading type. This data will identify the capacity limit in a wide variety of potential propagation scenarios. The ranging variance of the default system will also be analyzed as a function of SNR, fading type, and channel knowledge. Second, a new pilot placement will be examined where pilots are spaced every 8 subcarriers, yet the total pilot power remains the same. Communication capacity and ranging variance will be analyzed the same way as with the previous pilot placement. Third, the channel order and SNR will be fixed to analyze the impact that pilot spacing has on capacity. Last, the tradeoff between capacity and ranging variance will be examined as the power allocation between pilot and data subcarriers changes.

Since the modules operate with discrete signals, the integrals in the Ziv-Zakai bound computation were computed using a Riemann sum. To ensure accuracy of the Riemann sum, the signals were oversampled using a truncated sinc. Additionally, T_a is set as the length of one OFDM symbol. Since all parameters in Table I can be modified in the MATLAB modules, analysis can be performed by fixing certain parameters and sweeping others over a range. Note that carrier frequency is not a parameter. This analysis is strictly on signals that have already been down-converted to baseband by an analog front end. No carrier-phase information is used.

Note that (5) gives the communication capacity bound in units of bits-per-second-per-hertz (bps/Hz) and that (6) gives the Ziv-Zakai bound of the variance of ToA estimation in units of seconds-squared. To provide a more intuitive understanding of the Ziv-Zakai bound, the results will relate it directly to ranging error. Recall that for a ToA of τ seconds (s), the distance in meters (m) is given by $d = c\tau$, where c is the speed of light in meters-per-second (m/s). As such, the root-mean-square-error (RMSE) of the estimate d can be computed as:

$$\mathrm{RMSE} = c\sqrt{\mathrm{ZZB}} \tag{30}$$

RESULTS

In Fig. 1, pilots are placed every other subcarrier and the capacity is plotted against SNR. Power is equally allocated between all K subcarriers. The capacity curves are computed for AWGN and Rayleigh fading with channel orders of $L \in 0, 2, 4, 6$. AWGN achieves the highest capacity of all the fading environments. Under Rayleigh fading, the highest capacity is achieved for $L = 2$. As L increases up to $L = 2$, the diversity gain increases. However as L increases

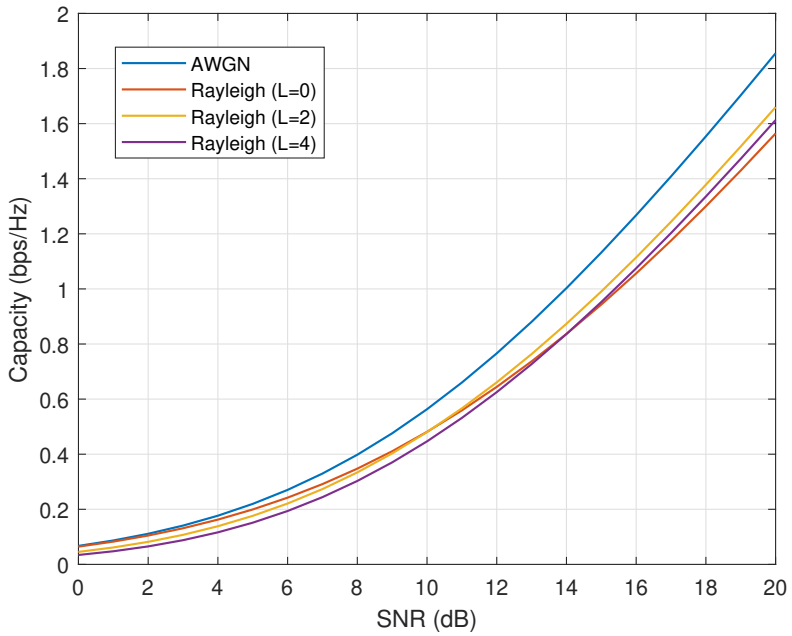

Fig. 1: The capacity bound for an 802.11a WiFi-like system with pilots placed every other subcarrier.

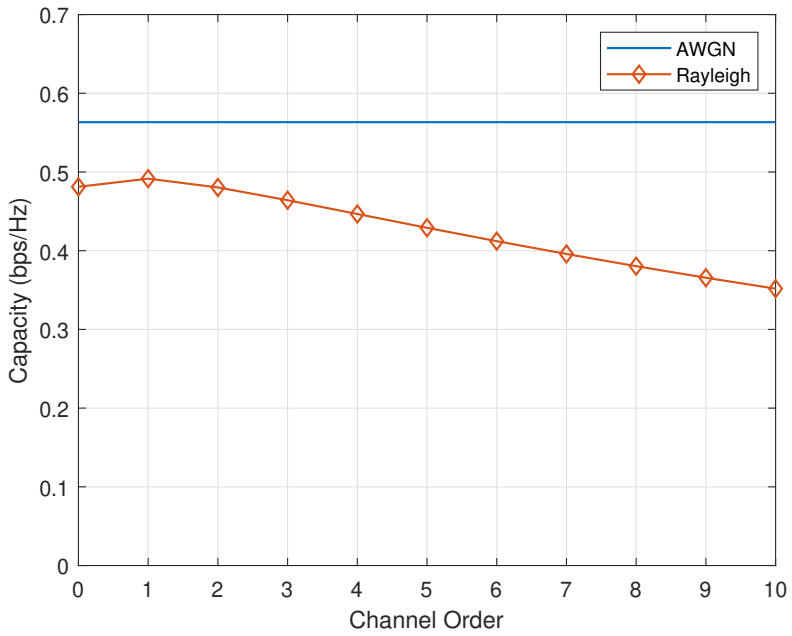

Fig. 2: The capacity bound for the same WiFi-like system at an average SNR of 10dB plotted against channel order.

beyond $L = 2$, the channel estimation error grows, counteracting any potential diversity gains at large channel orders. This phenomena is illustrated clearly in Fig. 2. In this figure, the SNR is fixed at 10dB. The AWGN scenario assumes a channel order of $L = 0$, so the line is extended across all channel orders for the sake of convenience.

Fig. 3 plots the Ziv-Zakai bound on RMSE ranging error against SNR for the same WiFi-like system with pilots every other subcarrier. The plot shows these curves for AWGN, Rayleigh fading with perfect channel knowledge and channel order $L = 0$, Rayleigh with perfect channel knowledge and channel order $L = 2$, Rayleigh fading with no channel

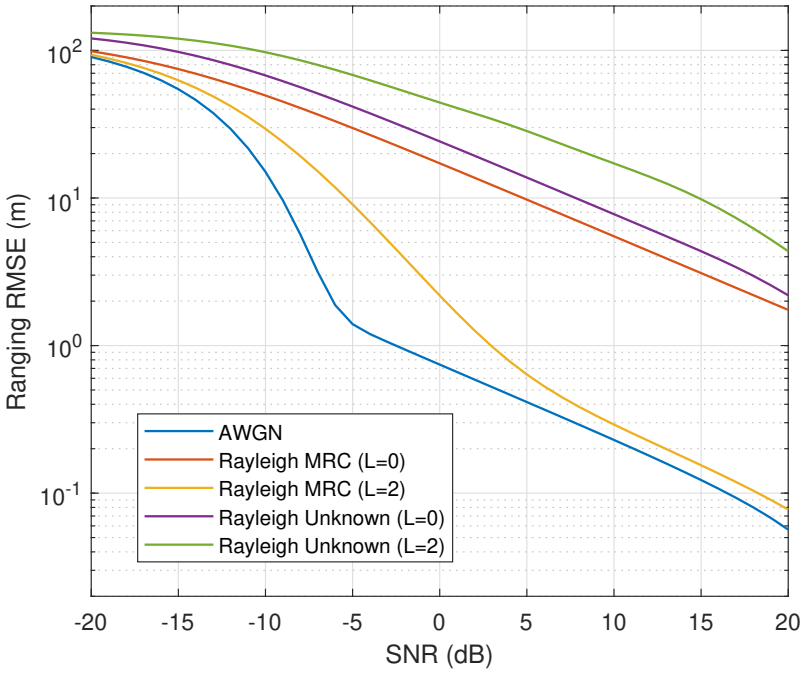

Fig. 3: The ranging variance bound for the same WiFi-like system with pilots placed every other subcarrier.

knowledge and channel order $L = 0$, and Rayleigh with no channel knowledge and channel order $L = 2$. In AWGN, the threshold effect occurs at -5dB, below which the RMSE increases toward the ambiguous RMSE. Under perfect channel knowledge, Rayleigh fading sees a higher bound on RMSE. However as the channel order increases, this curve approaches the AWGN curve, because the receiver experiences diversity gains. Under no channel knowledge, the curve is higher than the perfect knowledge case. When the channel order is increased, the no channel knowledge curve is pushed even higher. This is intuitive since the receiver experiences no diversity gain, and each channel tap has a smaller percentage of the total channel power.

Now the same WiFi-like system is modified to have a new pilot placement scheme where all pilot power (still half of the total signal power) is concentrated into the 2 outermost subcarriers. Fig. 4 fixes the SNR at 10dB and plots the capacity against channel order, much like in Fig. 2. Here, the plot shows that the capacity falls off monotonically with channel order. For Rayleigh $L = 0$, the system sees a greater capacity bound than that in Fig. 2. However, the capacity declines quickly and becomes less than Fig. 2 for $L \geq 3$. Fig. 5 shows the ranging RMSE bounds for the new pilot placement. Similar to before, AWGN has the lowest bound. Increases in the channel order push the Rayleigh fading curve with perfect channel knowledge toward the AWGN curve. The bounds for this pilot placement are much higher than that for the version in Fig. 3.

The next analysis looks at the impact that pilot spacing and the use of a preamble has on the capacity of the WiFi-like system. Fig. 6 plots capacity against the pilot spacing. The fading is Rayleigh with a channel order of $L = 6$. Power is allocated equally to all subcarriers regardless of the quantity used for pilot tones. In the first case, there is no preamble and only the data symbol with interspersed pilots is transmitted. In the second case, the transmitter sends one symbol with a Zadoff-Chu pilot sequence followed by the data symbol with interspersed pilots. Without the preamble, optimal pilot placement is achieved at a spacing of every 8 subcarriers. With the preamble however, the channel estimate is good enough that the pilots have little benefit and simply take up spectral resources that could be spent sending data. Since the capacity bound does not account for carrier-frequency-offset or common gain and phase error, this is expected. The insight gained from this plot is that under conditions where the channel must be estimated often, channel estimation can be performed effectively on pilots alone. However, this requires a large number of pilot tones to be more effective than a training preamble.

The last analysis performed is inspired by capacity region analysis in wireless communications. Namely, curves are plotted in the capacity-ranging variance space parameterized by the proportion of power allocated to the data tones, α.

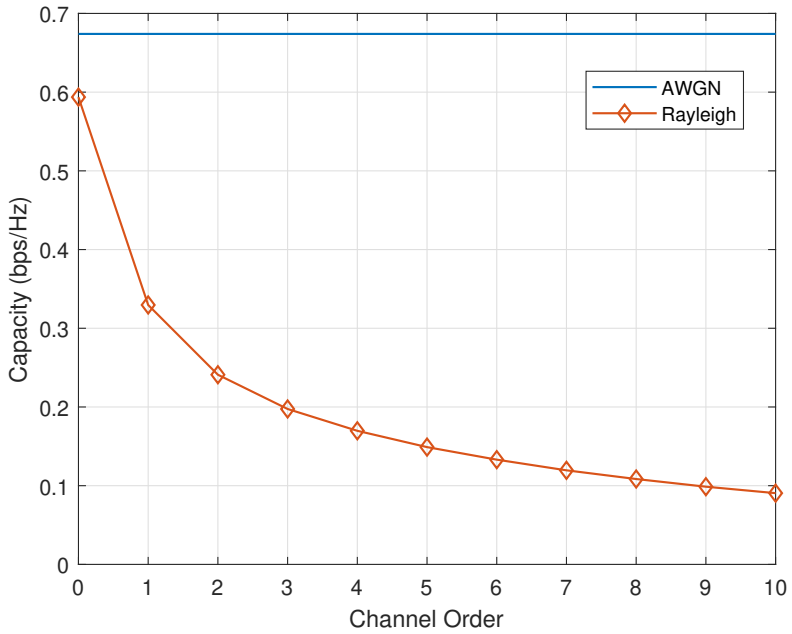

Fig. 4: The capacity bound for the same WiFi-like system, but with all pilot power put into the outermost 2 subcarriers, at an average SNR of 10dB plotted against channel order.

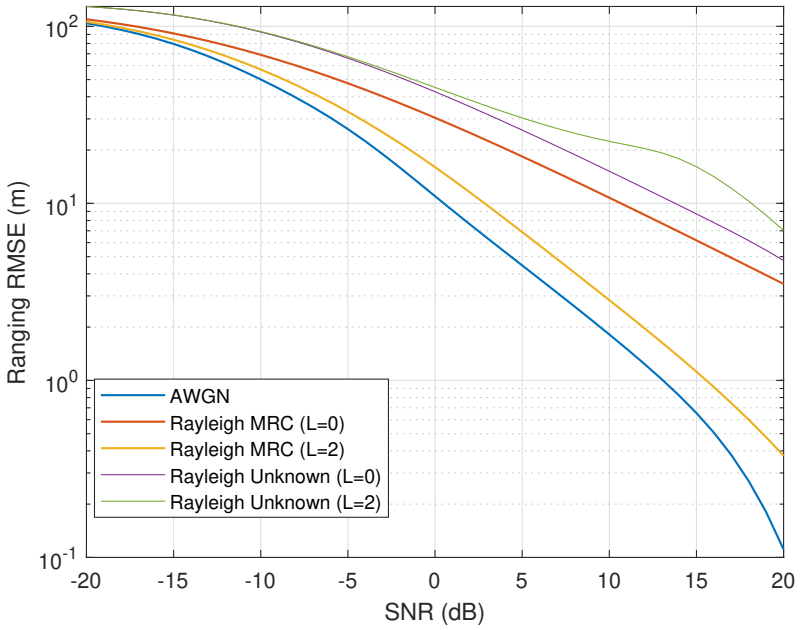

Fig. 5: The ranging variance bound for the same WiFi-like system, but with all pilot power put into the outermost 2 subcarriers.

Fig. 7 shows the achievable capacity-ranging variance pairs by varying α for a system with pilot spacing of $\Delta_P \in 2, 4, 8$ and a fixed SNR of 10 dB. The fading is Rayleigh with a channel order of $L = 7$. Tracing the outer-most curve gives the set of Pareto-optimal configurations. Given such a curve and an objective function in terms of the capacity and ranging variance to maximize, it is relatively straightforward to determine the optimal pilot spacing and power allocation as well as the resulting capacity and ranging variance. This plot signifies the important role that power allocation has,

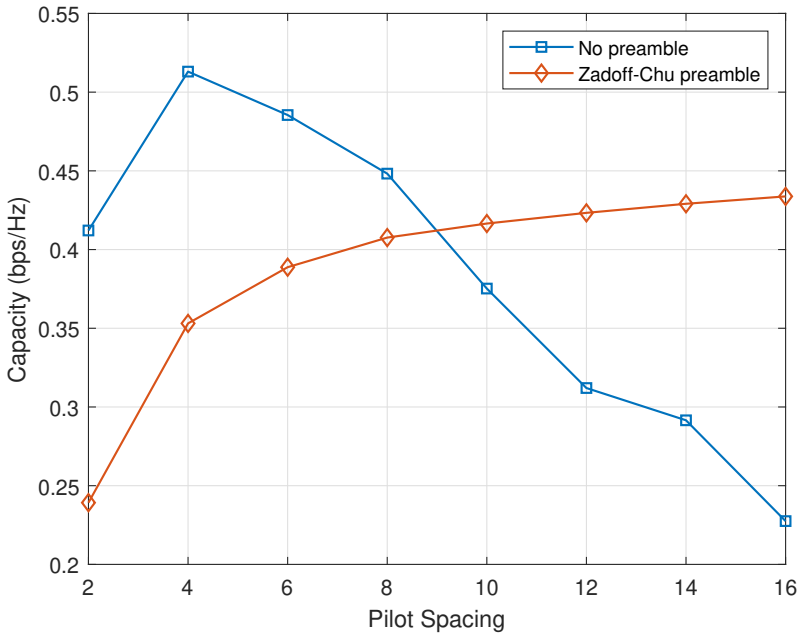

Fig. 6: The capacity bound for the same WiFi-like system but examining two variants. The first has no preamble, and every symbol is identical. The second is an extreme example that has a preamble place every other symbol. During the data symbols in both, pilots are equally spaced throughout. All subcarriers are allocated equal power. The channel order is $L = 6$.

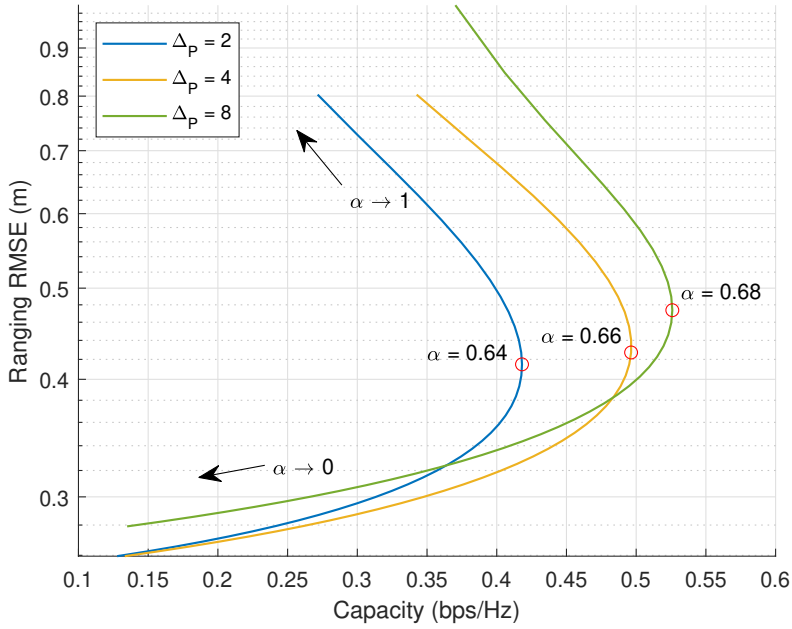

Fig. 7: Achievable capacity-ranging variance pairs by varying $\alpha \in (0.1, 0.9)$, the fraction of total power allocated to data subcarriers. Δ_P is the pilot spacing. SNR is fixed at 10 dB and the channel is Rayleigh fading with order $L = 7$. Perfect channel knowledge is assumed for computing the Ziv-Zakai bound.

and how it can be adapted to change both the communication capacity and ranging variance.

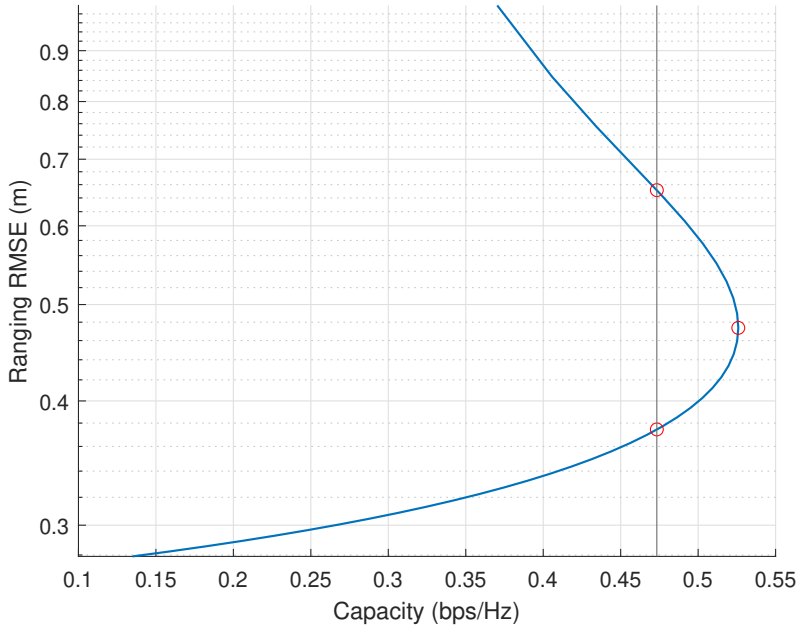

Fig. 8: Achievable capacity-ranging variance pairs by varying $\alpha \in (0.1, 0.9)$ with an added constraint on the capacity requirement. SNR is fixed at 10 dB, pilots are spaced 8 subcarriers apart, and the channel is Rayleigh fading with order $L = 7$. Perfect channel knowledge is assumed for computing the Ziv-Zakai bound.

As an example, consider the case where the system must minimize the ranging variance while simultaneously meeting a constraint that the channel capacity must be within 10% of the maximum channel capacity. As shown in Fig. 8, this constraint can be applied by drawing a vertical line at 90% of the maximum capacity (right-most point on the curve). The constrained minimum ranging variance can then be found by choosing the lowest point to the right of the vertical line. Due to the convexity of the capacity and ranging variance in this case, the variance is minimized on the intersection of the line and curve. This intersection can be used to determine the best choice of pilot spacing and power allocation.

CONCLUSION

In this paper, an analysis method was presented for upper-bounding the capacity and lower-bounding the ranging variance of an OFDM system as a function of the OFDM signal parameters. These bounds were derived for different propagation environments such as AWGN, frequency-flat Rayleigh fading, and frequency-selective Rayleigh fading. The bounds also accounted for both the thresholding effect experienced in ranging at low SNR and the capacity degradation caused by imperfect channel estimation. The utility of this method was shown for a simplified WiFi-like system. The impact that fading type, channel order, pilot placement, and power allocation has on this example system's capacity and ranging performance were displayed. Furthermore, an example of a constrained joint optimization was described and performed. This analysis enables simple and accurate joint optimization of OFDM schemes for both communication and ranging purposes.

ACKNOWLEDGMENTS

This work was supported by the U.S. Department of Transportation (USDOT) under Grant 69A3552047138 for the CARMEN University Transportation Center (UTC). It was also supported by affiliates of The University of Texas Wireless Networking and Communications Group.

REFERENCES

[1] 3GPP, "Study on NR positioning support," Tr 38.901, 3rd Generation Partnership Project (3GPP), March 2019, Version 16.0.0.

[2] Wang, D. and Fattouche, M., "OFDM Transmission for Time-Based Range Estimation," *IEEE Signal Processing Letters*, Vol. 17, No. 6, June 2010, pp. 571–574.

[3] Ziv, J. and Zakai, M., "Some lower bounds on signal parameter estimation," *IEEE Transactions on Information Theory*, Vol. 15, No. 3, 1969, pp. 386–391.

[4] Üreten, O. and Tascioundefinedlu, S., "Autocorrelation Properties of OFDM Timing Synchronization Waveforms Employing Pilot Subcarriers," *EURASIP Journal on Wireless Communications and Networking*, Jan. 2009.

[5] Wang, P. and Morton, Y., "Performance Comparison of Time-of-Arrival Estimation Techniques for LTE Signals in Realistic Multipath Propagation Channels," *Proceedings of the ION GNSS+ Meeting*, Sept. 2019, pp. 2241–2253.

[6] Shamaei, K. and Kassas, Z. M., "LTE receiver design and multipath analysis for navigation in urban environments," *NAVIGATION*, Vol. 65, No. 4, 2018, pp. 655–675.

[7] Shamaei, K., Khalife, J., and Kassas, Z. M., "Exploiting LTE signals for navigation: Theory to implementation," *IEEE Transactions on Wireless Communications*, Vol. 17, No. 4, 2018, pp. 2173–2189.

[8] Psiaki, M. and Slosman, B., "Tracking of Digital FM OFDM Signals for the Determination of Navigation Observables," *Proceedings of the ION GNSS+ Meeting*, Sept. 2019, pp. 2325–2348.

[9] Serant, D., Thevenon, P., Boucheret, M., Julien, O., Macabiau, C., Corazza, S., Dervin, M., and Ries, L., "Development and validation of an OFDM/DVB-T sensor for positioning," IEEE/Institute of Navigation, 2010, pp. 988–1001.

[10] Driusso, M., Comisso, M., Babich, F., and Marshall, C., "Performance Analysis of Time of Arrival Estimation on OFDM Signals," *IEEE Signal Processing Letters*, Vol. 22, No. 7, 2015, pp. 983–987.

[11] Wang, T., Shen, Y., and Mazuelas, S., "Bounds for OFDM ranging accuracy in multipath channels," *2011 IEEE International Conference on Ultra-Wideband (ICUWB)*, 2011, pp. 450–454.

[12] Goldsmith, A., *Wireless Communications*, Cambridge University Press, 2005.

[13] Yoo, T. and Goldsmith, A., "Capacity of fading MIMO channels with channel estimation error," *2004 IEEE International Conference on Communications*, Vol. 2, 2004, pp. 808–813.

[14] Tang, X., Alouini, M., and Goldsmith, A., "Effect of channel estimation error on M-QAM BER performance in Rayleigh fading," *IEEE Transactions on Communications*, Vol. 47, No. 12, 1999, pp. 1856–1864.

[15] Ohno, S. and Giannakis, G., "Capacity maximizing MMSE-optimal pilots for wireless OFDM over frequency-selective block Rayleigh-fading channels," *IEEE Transactions on Information Theory*, Vol. 50, No. 9, 2004, pp. 2138–2145.

[16] Dardari, D. and Win, M. Z., "Ziv-Zakai bound on time-of-arrival estimation with statistical channel knowledge at the receiver," *2009 IEEE International Conference on Ultra-Wideband*, 2009, pp. 624–629.

[17] Holm, H. and Alouini, M.-S., "Sum and difference of two squared correlated Nakagami variates in connection with the McKay distribution," *IEEE Transactions on Communications*, Vol. 52, No. 8, 2004, pp. 1367–1376.

[18] Joarder, A. H., "Moments of the product and ratio of two correlated chi-square variables," *Stat Papers*, Vol. 50, 2009, pp. 581–592.